Journal of Materials Chemistry C

ROYAL SOCIETY OF CHEMISTRY

PAPER

View Article Online
View Journal | View Issue

Cite this: J. Mater. Chem. C, 2023, 11, 8161

Star-shape non-fullerene acceptor featuring an aza-triangulene core for organic solar cells†

Yann Kervella,[a] José Maria Andrés Castán,[a] Yatzil Alejandra Avalos-Quiroz,[b] Anass Khodr,[b] Quentin Eynaud,[b] Tomoyuki Koganezawa,[c] Noriyuki Yoshimoto,[d] Olivier Margeat,[b] Agnès Rivaton,[e] Antonio J. Riquelme,[a] Valid Mwatati Mwalukuku,[a] Jacques Pécaut,[a] Benjamin Grévin,[a] Christine Videlot-Ackermann,[b] Jörg Ackermann,[b] Renaud Demadrille[a] and Cyril Aumaître*[a]

We present the simple synthesis of a star-shape non-fullerene acceptor (NFA) for application in organic solar cells. This NFA possesses a $D(A)_3$ structure in which the electron-donating core is an aza-triangulene unit and we report the first crystal structure for a star shape NFA based on this motive. We fully characterized this molecule's optoelectronic properties in solution and thin films, investigating its photovoltaic properties when blended with PTB7-Th as the electron donor component. We demonstrate that the aza-triangulene core leads to a strong absorption in the visible range with an absorption edge going from 700 nm in solution to above 850 nm in the solid state. The transport properties of the pristine molecule were investigated in field effect transistors (OFETs) and in blends with PTB7-Th following a Space-Charge-Limited Current (SCLC) protocol. We found that the mobility of electrons measured in films deposited from *o*-xylene and chlorobenzene are quite similar (up to 2.70×10^{-4} cm^2 V^{-1} s^{-1}) and that the values are not significantly modified by thermal annealing. The new NFA combined with PTB7-Th in the active layer of inverted solar cells leads to a power conversion efficiency of around 6.3% (active area 0.16 cm^2) when processed from non-chlorinated solvents without thermal annealing. Thanks to impedance spectroscopy measurements performed on the solar cells, we show that the charge collection efficiency of the devices is limited by the transport properties rather than by recombination kinetics. Finally, we investigated the stability of this new NFA in various conditions and show that the star-shape molecule is more resistant against photolysis in the presence and absence of oxygen than ITIC.

Received 20th December 2022,
Accepted 25th January 2023

DOI: 10.1039/d2tc05424h

rsc.li/materials-c

10th Anniversary Statement

Since the Journal of Materials Chemistry C was founded ten years ago, we have regularly published our work in this journal. Three years ago, I had the great honour of becoming one of its Associate Editors. For me and my co-workers, the Journal of Materials Chemistry C is one of the best journals in materials science because it publishes papers that propose new concepts and inspire new directions for research, especially in the field of organic (opto)-electrics and photonics. This journal brings together a large community of researchers in chemistry, physics and materials science. The synergy between these disciplines is very important for the development of cutting-edge research and technologies. I am pleased and proud to contribute to the development and growth of this journal and wish that it continues to play a leading role in the field of materials science. (R. Demadrille)

[a] *IRIG-SyMMES, Université Grenoble Alpes/CEA/CNRS, Grenoble, 38000, France. E-mail: cyril.aumaitre@cea.fr*
[b] *Aix Marseille Univ, CNRS, CINAM, Marseille, France*
[c] *Industrial Application Division, Japan Synchrotron Radiation Research Institute (JASRI), Sayo, Hyogo, 679-5198, Japan*
[d] *Department of Physical Science and Materials Engineering, Iwate University, Ueda, Morioka, 020 8551, Japan*
[e] *Univ. Clermont Auvergne, CNRS, SIGMA Clermont Inst. de Chimie de Clermont-Ferrand, UMR 6296 63000 Clermont-Ferrand, France*

† Electronic supplementary information (ESI) available. CCDC 2226762, 2226763 and 2226764. For ESI and crystallographic data in CIF or other electronic format see DOI: https://doi.org/10.1039/d2tc05424h

Introduction

Organic photovoltaics (OPVs) have attracted significant interest from the scientific community and companies for more than three decades due to their unique advantages compared to their inorganic counterparts.[1] Organic solar cells (OSCs) use ultra-thin layers of organic semiconductors allowing the fabrication of lightweight, flexible and even semi-transparent devices. They can be manufactured at the industrial scale using low-cost

printing methods, thus reducing their carbon footprint.[2] Until the middle of the 2010s, OSCs' performances have continuously progressed thanks to the development of a large library of p-type polymers.[3] These polymers have been mostly used with fullerene-based materials, such as phenyl-C_{61}-butyric acid methyl ester ($PC_{61}BM$) or its C_{70} analogue ($PC_{71}BM$). In such systems, photons are mainly absorbed by the polymer and not by the fullerene, thus limiting power conversion efficiency (PCE). In 2013, Nelson and Janssen identified the factors limiting the device efficiency in OPV and predicted that PCE of over 20% could be reachable in single junctions.[4] Since then, considerable efforts have inspired new research directions in semiconductors synthesis,[5] device engineering,[6,7] and tandem or ternary approach.[8,9] Swapping fullerenes for other molecules in bulk-heterojunction solar cells has been a challenge. In recent years, the rise of non-fullerene acceptors (NFAs) resulted in quick improvements in device efficiency and opened new perspectives for the launch of this technology in building integrated photovoltaics.[10] The development of molecules such as ITIC derivatives, followed by the Y6 family, led to a rapid increase in the performances, which attained 19.2% in 2022, which would have been unthinkable a few years ago.[11–14] The performances of OSCs are now competitive with well-established technologies such as silicon solar cells, but their long-term stability and the development of even more ecological fabrication process still require research efforts.[10,15–17] In comparison to the plethora of linear NFA molecules developed in the last decade, only a few efficient star-shaped NFAs have been reported in the literature.[18,19] Star shape molecular semi-conductors containing donor and acceptor units have attracted increasing attention for use in OLEDs since many of them show thermally activated delayed fluorescence (TADF) characteristics.[20,21] However, the potential of donor–acceptor star-shape NFAs for application in OSCs remains underexplored despite some demonstrating PCE over 10%.[22]

Star shape NFAs show some advantages compared to linear systems, such as their 3D structure that promotes an isotropic charge transport or lowers the aggregation propensity that can enhance the nanoscale phase separation in thin films.[22] The main families of star shape molecules comprise spiro-fluorene,[22] perylene diimide,[23–25] a triphenylamine (TPA) or truxene core.[26–29] We learn from previous works that the bulkiness of the truxene core, which comes from the alkyl side chains, limits the molecular aggregation and tends to stabilize the morphology.[29] Unfortunately, truxene is rather sensitive to photo-oxidation, which can lead to rapid performance degradation.[30] The TPA unit has often been used as a core to design star-shape NFAs leading to increased exciton dissociation efficiency in blends. Unfortunately, the TPA unit's poor rigidity and the molecule's strong distortion can be detrimental to the transport and impact the blends' thermal and morphological stability.[22]

To solve these problems, Xiong *et al.* have proposed the synthesis of an NFA molecule based on a fused-TPA core, also known as aza-triangulene.[31] This molecule was coupled with 3 perylene diimide acceptor units through dimethylmethene-spacers (DMTPA-PDI3). This molecular design induced a better π-electron delocalization resulting in a wider spectral absorption and a higher LUMO level. When used in blend with PTB7-Th, this star shape NFA shows a low intermolecular aggregation, giving rise to a uniform bulk-heterojunction and a balanced charge transport. To the best of our knowledge, DMTPA-PDI3 is the only example containing an aza-triangulene central unit in the construction of star shape NFA materials, leading to a PCE of 5% when used with PTB7-Th.

Our interest in aza-triangulene-based molecules not only comes from their better optical properties and lower propensity to aggregate when mixed with polymers but also from their remarkable electrochemical stability. Compared to TPA-based molecules, the central sp^3-nitrogen of aza-triangulene is shielded by the substituents attached to the carbon bridge linking the phenyl units.[32,33] This helps stabilizing molecules either in the neutral or even in their oxidized states.[34]

Surprisingly, only a few examples of small molecules based on an aza-triangulene core have been reported for use in bulk-heterojunction solar cells, mainly as donor components.[35–37]

To explore further the potential of star shape NFA molecules based on an aza-triangulene core in organic solar cells, in this work, we designed and synthesized a novel star shape NFA embedding an aza-triangulene unit functionalized by 3 electron accepting units based on 2-(3-oxo-indan-1-ylidene)-malononitrile groups. These accepting groups are connected to the central unit through a thiophene-vinylene bridge. We report the crystal structure of this molecule, being the first one reported so far for a star shape molecule based on an aza-triangulene unit. Then, we investigate its optoelectronic and transport properties in detail, and report its photovoltaic performances in blend with PTB7-Th (deposited from non-chlorinated solvent) leading to a maximum PCE of 6.27%. We identify the factors limiting the efficiency of this molecule in devices thanks to impedance spectroscopy measurements and, finally, we study its degradation mechanisms.

Results and discussion

Synthesis

The synthesis of the **AzaTk** NFA is shown in Fig. 1. First, the aza-triangulene core was synthesized in 2 steps following literature procedures (see ESI†).[38] Then, with the double goal of enhancing the solubility in non-halogenated solvents and increasing the steric hindrance around the nitrogen core, six phenylhexyl units were introduced on the sp^3-spiro bridges. The core was brominated in 3 positions with NBS and **TriAld** was then obtained from this intermediate in an 88% yield *via* a Stille cross-coupling reaction followed by an acidic deprotection. **AzaTk** was finally obtained in good yield (85%) through a Knoevenagel condensation. It has to be highlighted that the new NFA can be obtained with a remarkable overall yield of 28%.

After the purification of the **AzaTk** molecule, we obtained crystals suitable for X-ray crystallographic analysis (Fig. 1b) by vapour diffusion method in a dibromomethane/cyclohexane mixture. From the X-Ray structure, we confirm the planarization

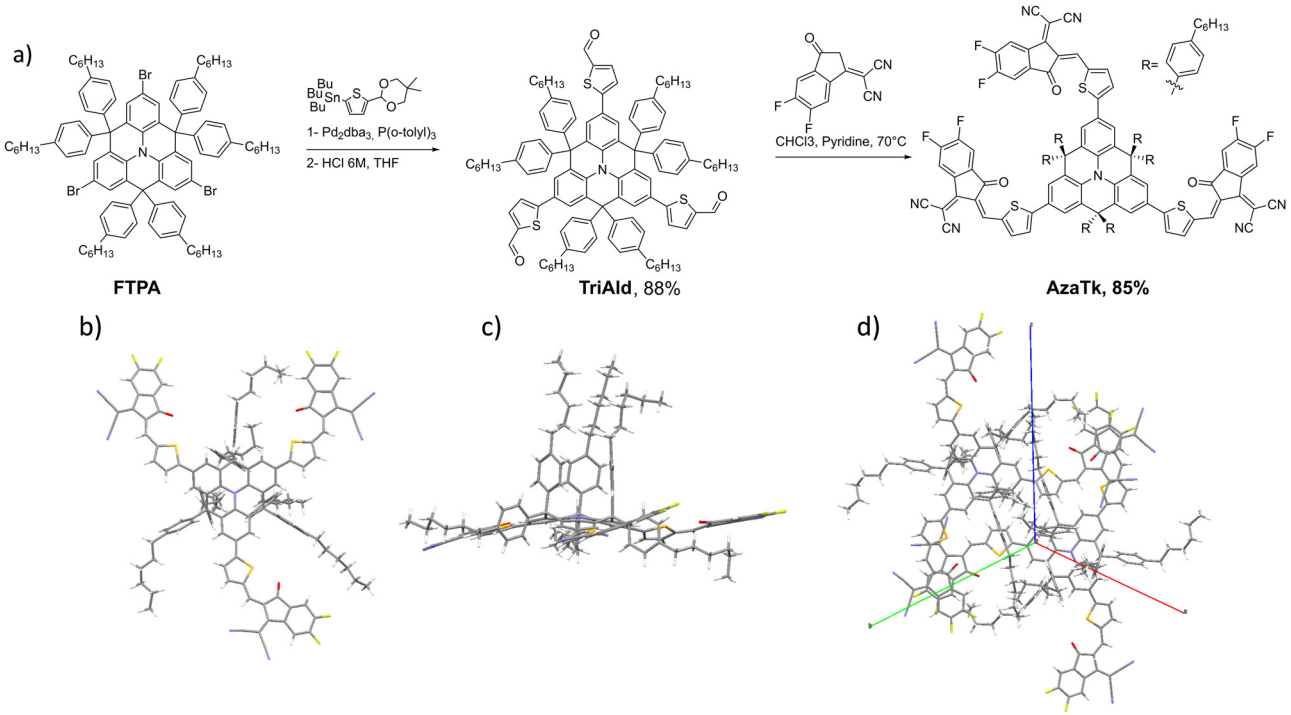

Fig. 1 (a) Synthesis of **AzaTk** non fullerene acceptor. X-Ray structure of the **AzaTk** molecule (b) top view, (c) side view, (d) crystal-packing.

of the triphenylamine core.[34] We clearly see that the hexylphenyl units on the sp^3 carbon are oriented in the axial and the equatorial positions leading to the formation of a ''cage'' around the nitrogen atom of the central electron-rich unit. The vinylene bridges are all oriented in *cis* configuration with the cyano groups pointing outwards of the core. The close interactions between the oxygen and sulfur atoms planarize the extremities without preferential orientation for the thiophene linked to the core. One should also mention that the distance between the electron accepting units of two different molecules in the crystal is 3.37 Å, which is typical for pi-stacking interactions.

Optical properties

The NFA was found to be soluble in the main chlorinated solvents used for the processing of OPV devices, such as chloroform and chlorobenzene (CB), but also in the more industrial friendly *o*-xylene. The absorption spectra measured in chlorobenzene and *o*-xylene are collected in Fig. 2.

In solution, the molecule shows a broad absorption band across the visible spectrum with a maximum found at 642 nm (CB) and 630 nm (*o*-xylene) corresponding to the HOMO–LUMO transition (see TDDFT absorption simulation in Fig. S1 and S2, ESI†), the maximum molar absorption coefficient of this band was found to be 1.28 10^5 L mol^{-1} cm^{-1} in chloroform (Fig. S3, ESI†). Compared to the CB solution, the absorption peak of **AzaTk** in *o*-xylene is blue-shifted. It may be attributed to the different polarity index of both solvents.[39] This value lies in the same range as those of other NFA materials, such as ITIC or Y6, and materials made of the same central core.[35,40,41] In addition, **AzaTk** also presents an additional absorption band at *ca.* 475 nm corresponding to other optical transitions with higher energy. Thanks to TDDFT theoretical calculation, we mainly identified the contribution of the HOMO−1 → LUMO and

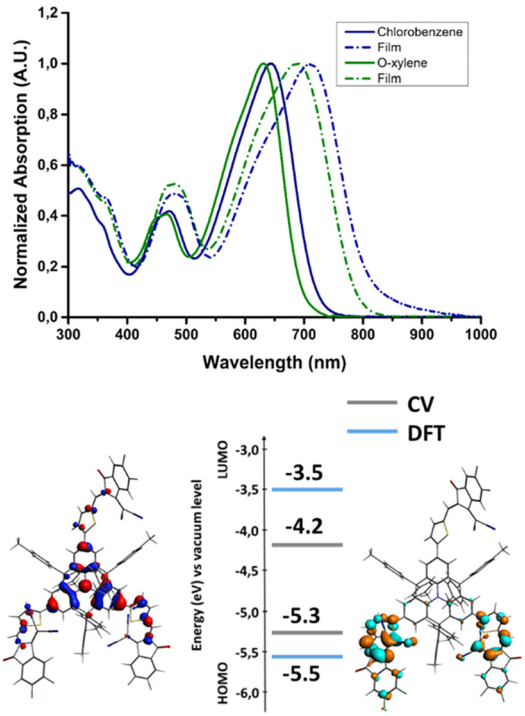

Fig. 2 Absorption spectra of **AzaTk** in solution and in thin films. Energy levels and electron density of the HOMO (left) and LUMO (right) of **AzaTk** obtained by cyclic voltammetry and DFT calculations.

HOMO−1 → LUMO+1 transitions for this band which correspond to a more localized internal charge transfer between the π-conjugated bridge and the acceptor units (see Fig. S2, ESI†). We highlight that this absorption band is not present in others NFA materials (*vide supra*) and maximizes the photon collection in this part of the visible spectrum. Then, once deposited by spin coating from *o*-xylene and chlorobenzene solutions, a bathochromic shift of respectively 66 and 56 nm is observed when compared to the spectra in solution. No significant difference between both films was observed, leading to a similar bandgap (1.55 eV). Also, we do not observe any shoulder peak corresponding to aggregation generally observed for other NFAs. It could come from the hindered 3D structure of **AzaTk** inhibiting crystallization or aggregation in thin films.[42] In addition, no significant differences were observed after a 10 minutes annealing process at 100 °C was carried out.

To look deeper into the electronic properties of **AzaTk**, we analyzed the molecule's energy levels through cyclic voltammetry experiments and DFT calculation (Fig. 2). The measurements were carried out in dichloromethane with $Ag/AgNO_3$ as a reference electrode and Fc/Fc^+ couple as an internal reference. The highest occupied molecular orbital (HOMO) and the lowest unoccupied molecular orbital (LUMO) were determined respectively from the onset oxidation and reduction potentials (see Fig. S4, ESI†). In oxidation, a first reversible oxidation followed by a quasi-reversible peak was observed. In reduction, an irreversible reduction was measured, leading to the decomposition of the material. **AzaTk** shows HOMO and LUMO levels located at −5.3 and −4.2 eV, respectively, *versus* the vacuum level. In parallel, DFT theoretical calculations were carried out, giving calculated HOMO at −5.5 eV and LUMO at −3.5 eV. In the ground state, the electron density is mainly localized on the aza-triangulene core with a slight extension to the lateral thiophenes due to the low dihedral angle (20°) observed in the crystal structure. For the LUMO localization, the electron density is shifted to the accepting unit and distributed only over the two branches.

This spatial repartition has been observed with other star shape structures. It is often considered as degenerated energy levels (LUMO and LUMO+1) due to the splitting of the ICT transition from the central core to the three branches (see ESI†).[26,31]

Transport properties

In order to gain first insight into the transport capacity of the pristine new material itself, we fabricated organic field effect transistors (OFETs) in BGBC configuration (see ESI†). Both chlorinated and non-chlorinated solvents were used to process thin films of **AzaTk** molecule under an inert atmosphere through spin-coating. The results are compared with the ITIC-Th molecule, which is known to be an excellent acceptor material with PTB7-Th in binary blends.[41] The results are reported in Table S1 (ESI†). By applying the same treatments to OTFTs as we did previously for ITIC-Th (see SI for details), namely modified gold electrodes and passivated dielectric layer, a perfectly unipolar electron transport is observed proving that the new **AzaTk** molecule is an n-type material. This is highlighted by an accumulation mode in positive bias together with a depletion in negative bias (Fig. S5, ESI†). Although the injection is slightly disturbed by the presence of the coating passivating the electrodes, as it can be seen from the slower current rising at low voltages, OTFTs deliver a high drain current in the saturation regime with a well-defined accumulation. Similar electron mobility values were observed for films cast at room temperature from *o*-xylene and CB solutions of 1.1×10^{-4} and 1.2×10^{-4} $cm^2\ V^{-1}\ s^{-1}$ respectively. Post-annealing of the layers up to 200 °C leads only to small variations of the electron mobilities as shown in Table S1 (ESI†) demonstrating the low impact of the thermal annealing process on mobility values. Thermogravimetric analysis of **AzaTk** under nitrogen has shown that no degradation is observed before 330 °C (Fig. S6, ESI†). This suggests that **AzaTk** molecular organization little depends on the processing conditions, and encourages the use of a simple as-cast process which is more compliant with industrial requirements. Compared to ITIC-Th, the mobility value is one order of magnitude lower, but at the same time still in the same range as the hole mobility measured for PTB7-Th at 1.5×10^{-4} $cm^2\ V^{-1}\ s^{-1}$ (Fig. S7, ESI†), which should be beneficial for the performances of OSCs.[43,44]

In a second approach to evaluate the vertical transport capacity of both materials involved in bulk heterojunctions, we used a Space-Charge-Limited Current (SCLC) protocol to extract the mobility from *I–V* curves of hole-only and electron-only devices (see experimental part). Bulk heterojunctions were realized with the same procedure used in photovoltaic devices (*vide infra*) by mixing the **AzaTk** molecule with the PTB7-Th donor polymer with a 1 : 1 weight ratio in CB and *o*-xylene. *I–V* curves were fitted in the SCLC region considering a field-dependence of the mobility. Hole (μ_h) and electron (μ_e) mobility values obtained for PTB7-Th:**AzaTk** BHJ layers as a function of solvent are summarized in Table S2 (ESI†). Fig. S8 (ESI†) shows representative dark current and fitting curves. Based on hole-only devices, the hole mobility is slightly higher for CB with average values of 8×10^{-4} *vs.* 3.1×10^{-4} $cm^2\ V^{-1}\ s^{-1}$ for *o*-xylene, suggesting a morphological influence of the PTB7-Th chains arrangement in BHJs. For both solvents, the electron mobility in PTB7-Th:**AzaTk** blended films is lower with average values of 6.5×10^{-5} and 1.9×10^{-6} $cm^2\ V^{-1}\ s^{-1}$ for CB and *o*-xylene, respectively. However, this result indicates that despite the presence of polymer chains surrounding the **AzaTk** domains, the electron transport pathways persist throughout the entire volume of the layer. Additionally, the electron mobility of blends processed from *o*-xylene is clearly lower leading to a more unbalanced hole and electron mobility that increases the build-up of space charges and, hence, may, increase charge recombination. (*vide infra*)

Photovoltaics properties

Among the wide choice of p-type donor polymers, we chose PTB7-Th as the donor due to its more suitable energy levels (HOMO: −5.2 eV and LUMO: −3.7 eV) to the levels of **AzaTk** *i.e.*, HOMO: −5.3 eV LUMO: −4.2 eV. The absorption spectra of PTB7-Th:**AzaTk** blended films are shown in Fig. 3. Due to the

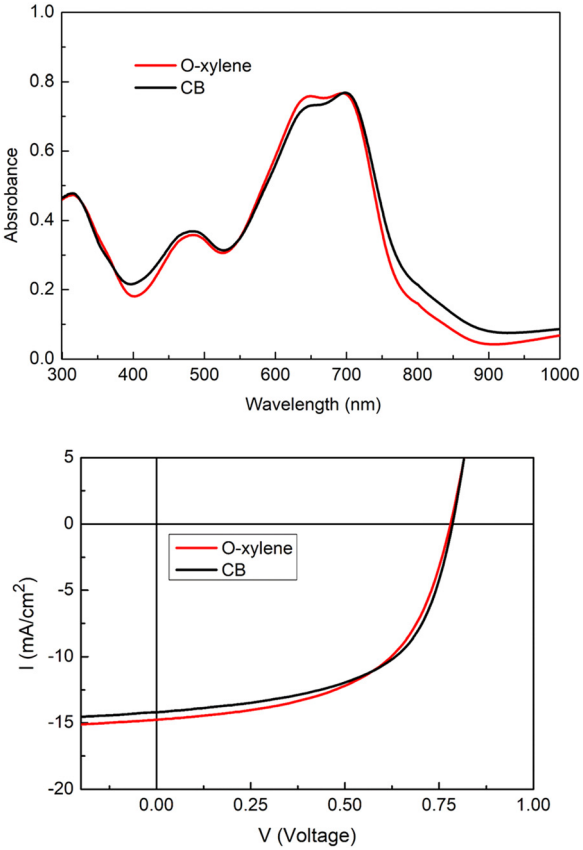

Fig. 3 Absorption spectra and *I*–*V* curves of PTB7-Th:**AzaTk** blend film deposited from *o*-xylene and chlorobenzene solutions.

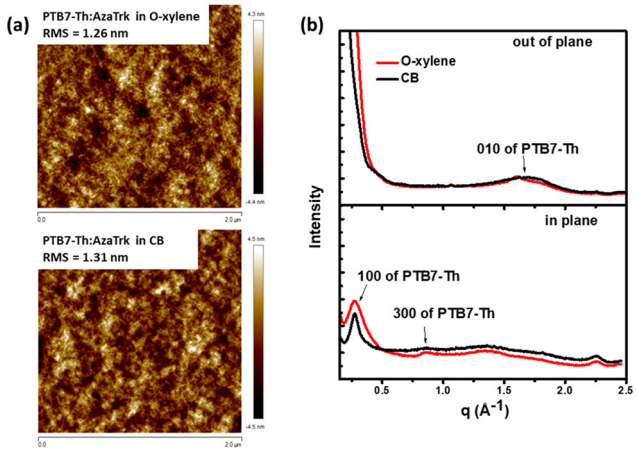

Fig. 4 AFM images (a) and (b) 2D-GIXRD profiles in out of plane and in plane of line cuts of PTB7-Th:AzaTk blend films from *o*-xylene and chlorobenzene solutions.

overlapping absorption of the two compounds, the blend absorption is centered between 550 and 850 nm. Films cast from *o*-xylene and chlorobenzene (97% CB/3% CN) were implemented as an active layer in inverted device structure (glass/ITO/ZnO/PTB7-Th:**AzaTk**/MoO_3/Ag) to evaluate the photovoltaic properties of **AzaTk**-based acceptor. A reference system PTB7-Th:ITIC-Th was selected and we applied identical process parameters for both blends, with a D : A ratio of 1 : 1 in a total concentration of 20 mg mL^{-1} in 97% CB/3% CN. The current density–voltage (*J*–*V*) curves are shown in Fig. 3 and the photovoltaic parameters are summarized in Table 1. Slightly better performances were obtained with chlorobenzene due to a better FF. The highest efficiency was obtained for the inverted configuration using chlorobenzene solution with a PCE of 6.46% and a J_{sc} of 14.09 mA cm^2. Remarkably, V_{oc} remains identical, independent of the solvent used, with a value of 0.78 V. For the blend processed from *o*-xylene solution, the PCE drops to 6.27% despite a higher Jsc. These PCE values are quite comparable and clearly lower compared to the PCE of 8.7% of the reference cells based on PTB7-Th:ITIC-Th. The loss in performance compared to the ITIC-Th based devices can be correlated to the narrower spectral absorption range in the PTB7-Th:**AzaTk** mixture compared to PTB7-Th:ITIC-Th. The lower absorption leads to a lower J_{sc}. The poorer FFs can be explained by the lower electron mobility of **AzaTk** acceptor inside the blend leading to unbalanced charge extraction.

The EQE spectra of both devices show an identical profile of photoconversion efficiency in the whole range from 300 to 900 nm matching well the absorption of PTB7-Th:**AzaTk** blend films (see Fig. S9, ESI†). This indicates that in both cases PTB7-Th and **AzaTk** contribute identically to the photocurrent generation.

Morphological studies

As the morphology of the active layers at the nanoscale has a strong influence over the exciton dissociation and the charge transport, we conducted first atomic force microscopy (AFM) study on PTB7-Th:**AzaTk** blend in *o*-xylene and chlorobenzene together with ITIC-Th:PTB7-Th as the reference (Fig. 4 and Fig. S10, ESI†). Both films exhibited smooth and uniform

Table 1 Photovoltaic parameters of PTB7-Th:**AzaTk** blend in o-xylene and chlorobenzene and PTB7-Th:ITIC-Th blend as a reference. Statistical values are calculated from the mean of 3–5 cells. The active area is 0.16 cm^2. Hole and electron mobilies measured for thin film deposited as cast in SCLC configuration. (see ESI for more informations)

	V_{OC} (V)	J_{SC} (mA cm^{-2})	FF (%)	PCE (%)	$\mu_{hole(SCLC)}$ (cm^2 V^{-1} s^{-1})	$\mu_{electron(SCLC)}$ (cm^2 V^{-1} s^{-1})
PTB7-Th:**AzaTk** *o*-Xylene	0.78 ± 0.002	14.43 ± 0.22	55.43 ± 0.31	6.27 ± 0.07	3.10×10^{-4}	1.89×10^{-6}
PTB7-Th:**AzaTk** Chlorobenzene	0.78 ± 0.002	14.09 ± 0.09	58.33 ± 1.00	6.46 ± 0.06	8.01×10^{-4}	6.54×10^{-5}
PTB7-Th:ITIC-Th Chlorobenzene	0.79 ± 0.002	16.65 ± 0.11	59.92 ± 1.4	8.70 ± 0.26	—	—

surface morphology, similar to those of PTB7-Th:ITIC-Th blends, with root-mean-square (RMS) roughness around 1–2 nm. This result confirms the good miscibility of the new acceptor with donor polymer when deposited either from a chlorinated (chlorobenzene) or a non-chlorinated (*o*-xylene) solvent. Additionally, this highlights the efficacy of star shape NFA to restrain intermolecular aggregation and favors uniform domains. To further explore the organization of **AzaTk** inside the blend, we compared the out-of-plane and in-plane GIXRD profiles of PTB7-Th:**AzaTk** films at ratio 1 : 1 proceed from *o*-xylene and CB solutions in Fig. 4(b). The corresponding 2D-GIXRD patterns are provided in Fig. S11 (ESI†). Both diffraction scans show the in-plane (100) reflection and the broad out-of-plane (010) reflection of PTB7-Th, which indicates the typical face-on orientation of PTB7-Th crystals (the scattering of the corresponding neat PTB7-Th film is shown in Fig. S12, ESI†).[45] However, there are no additional peaks in the blend diffraction patterns that can be attributed to **AzaTk** molecules pointing towards a lack of order of the new acceptor in the blend, while the preferential arrangement of PTB7-Th polymer chains in a thin layer is not modified. However, the position of the peak (100) corresponding to the lamellar packing of PTB7-Th changes slightly from 0.256 $Å^{-1}$ (d = 24.53 nm) for the neat polymer film to 0.28 $Å^{-1}$ (d = 22.42 nm) and 0.278 $Å^{-1}$ (d = 22.58 nm) for PTB7-Th:**AzaTk** films proceed from *o*-xylene and CB, respectively. Smaller lamellar packing distances in blends highlight an improved molecular packing of PTB7-Th due to the presence of acceptor molecules. This favorable arrangement of PTB7-Th chains could explain the higher hole mobility observed in blends. The crystal coherence length (CCL) was estimated from the full width half maxima (FWHM) of peaks by using the Scherrer equation (eqn (1) in ESI†).[46] CCL is calculated to be between 0.82 and 0.85 nm for the neat PTB7-Th film and PTB7-Th:**AzaTk** blend proceed from *o*-xylene, and it increases to 1.3 nm for PTB7-Th:**AzaTk** blend proceed from CB. The π–π stacking peak (010) of PTB7-Th is shown at q = 1.55 $Å^{-1}$ (d = 0.405 nm) in Fig. S12 (ESI†) and goes to q = 1.605 $Å^{-1}$ (d = 0.391 nm) and q = 1.701 $Å^{-1}$ (d = 0.369 nm) for PTB7-Th:**AzaTk** films proceed from *o*-xylene and CB, respectively (Fig. 4b). This confirms that the molecular packing of PTB7-Th is much denser in blended films processed with CB. The vertical π–π stacking is well-known to promote charge transport between anode and cathode of solar cells and corroborates the higher hole mobility values observed by SCLC for blends using CB. A slight increase in device performances, particularly the FF, is subsequently observed.

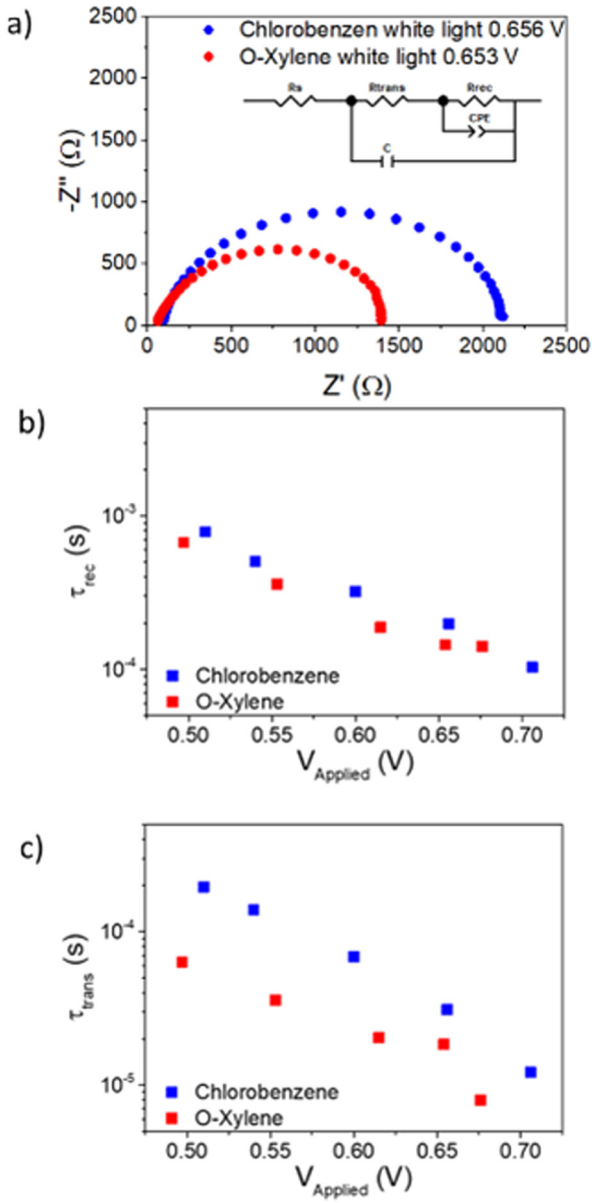

Fig. 5 (a) Nyquist spectra from impedance measurements of aza-triangulene-based organic solar cells using *o*-xylene and chlorobenzene as solvents under white illumination. Equivalent circuit used to fit the resulting spectra included as inset. Recombination lifetime (b) and electron diffusion transit time (c) extracted from the impedance spectra of aza-triangulene-based organic solar cells using *o*-xylene and chlorobenzene as solvents under white illumination, applying the equivalent circuit depicted in the inset of (a).

Impedance spectroscopy

To cast light on the recombination and transport properties of OPV devices, electrical impedance spectroscopy has widely been used.[47–51] These measurements were performed on devices using films formed as cast from chloroform and *o*-xylene solutions using a Thorlabs white LED in a wide range of DC light intensities under ambient conditions. Typical Nyquist spectra obtained for the chlorobenzene and *o*-xylene devices in these experiments are shown in Fig. 5.

The resulting Nyquist spectra were fitted using the equivalent circuit included as inset in Fig. 5(a).[47,48,52,53] In this circuit, R_S accounts for the series resistance of the system, R_{trans} and R_{rec} are the transport and recombination resistances, respectively, C is the device dielectric capacitor and CPE is a constant phase element acting as chemical capacitor produced by photogenerated charge accumulation.[54] The values of the other elements included in the equivalent circuit as a function of the applied voltage can be observed in Fig. S13 (ESI†).

The resulting resistances and capacitances can be used to determine the recombination lifetime or average charge carrier

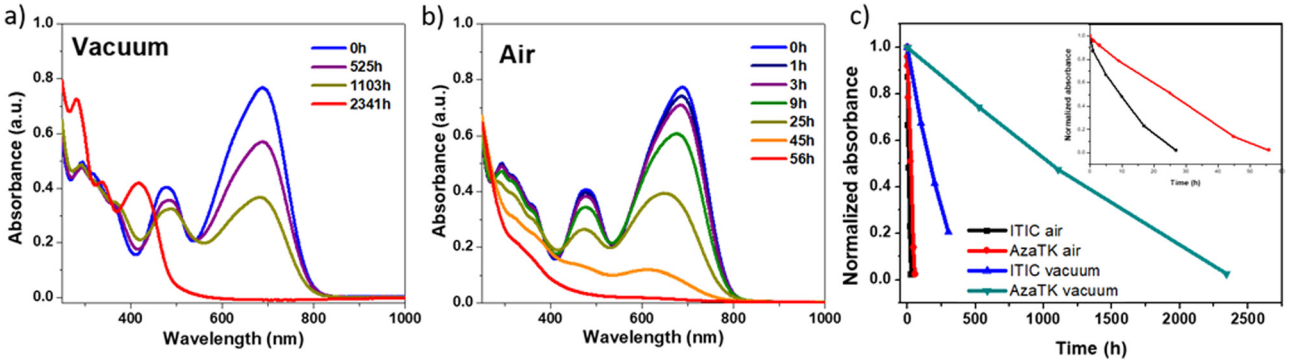

Fig. 6 Absorbance spectra of the evolution of the **AzaTk** molecule under constant illumination using simulated AM1.5 light in (a) absence of oxygen (vacuum) and (b) presence of oxygen (air). (c) degradation kinetics of both mechanism of **AzaTk** compared to reference ITIC molecule.

lifetime (τ_{rec}) can be calculated using the following expression[49,55]

$$\tau_{rec} = R_{rec} \cdot C_{chemical} \quad (1)$$

Similarly, the electron diffusion transit time (τ_d) can be calculated using the equation below[49,51]

$$\tau_{trans} = R_{trans} \cdot C_d \quad (2)$$

By applying eqn (1) and (2) to the corresponding resistances and capacitances, the recombination lifetime and the electron diffusion transit time were extracted and presented in Fig. 5(b and c).

Attending to Fig. 5(b), both devices show similar recombination lifetimes, which is in agreement with the equal values of the V_{OC} for both kinds of devices. On the other hand, in panel (c) it can be observed how the electronic transport is significantly faster, which can explain the higher J_{SC} produced by the *o*-xylene based device limiting its charge collection efficiency.[56,57] This suggests that the charge collection efficiency of these devices is limited by the transport properties rather than by recombination kinetics.[58]

Photostability and photo-oxidation studies

In the last few years, efforts have been made to push further the performances of organic solar cells, but more importantly, it is crucial to tackle the challenge of their long-term instability. To further characterize **AzaTk** and understand the molecule's behavior under specific environmental conditions related to their application in OPV, analysis of the photo-degradation process in the absence (photolysis) and presence (photo-oxidation) of oxygen were performed. Pristine films of **AzaTk** deposited on glass and KBr substrates were subsequently exposed to simulated AM1.5 light at 1000 W m^{-2} and a 400 nm UV light filter was used to avoid the effect of high energy photons. The time evolution of the film degradation was monitored by absorbance in Fig. 6 and IR spectra in Fig. S15 (ESI†) in both, air and vacuum conditions. For comparison purpose we use ITIC as a reference material, since its degradation has already been the subject of several articles.[59,60] We followed its degradation in the absence and presence of oxygen (see Fig. S16, ESI†). In the absence of oxygen, ITIC shows almost complete degradation after only 300 h under continuous illumination, whereas **AzaTk** molecule retains 80% of its initial absorbance in the same time period as seen from the curves in Fig. 6(c). **AzaTk** molecule is clearly more stable under inert atmosphere compared to ITIC. ITIC and **AzaTk** have in common the same acceptor moieties in which a photo-isomerization rearrangement can occur. In order to confirm that the photo-degradation process identified by Perepichka *et al.* can occur with **AzaTk**, we left **AzaTk** chloroform solution under ambient light and managed to isolate the by-products formed in solution after chromatography column. Absorption spectra and ^{1}H NMR were carried out on the most abundant species and the spectra are shown in Fig. S18 (ESI†).

We found that by-products similar to those reported for ITIC are formed.[60] **AzaTk** contains fluorinated end-groups as previously observed on other NFA molecules BITIC-C_8F_4 and BITIC-PhC_6F_4, and the presence of fluorine substituents seems to have a positive effect on the intrinsic stability of the NFAs.[8]

In the case of the photo-oxidation (Fig. 6(b)), degradation is much faster and the **AzaTk** film withstands only 56 h of illumination before degrading completely. Compared with ITIC, **AzaTk** retains, however, more than 75% of the initial absorbance after 10 h, while ITIC films lose 50% of its initial absorption indicating a superior stability against photo-oxidation. Compared to **AzaTk**, the absorption maxima of the degraded product is blue-shifted by 140 nm (0.11 eV) which is accounted by the breaking of the conjugated backbone between the aza-triangulene core and the dicyanomethylene accepting group. Also, the ^{1}H NMR spectrum of the degradation product features an sp^3 singlet around 4.5 ppm which is in the same range as the ITIC-4F degradation product observed by Perepichka group.

To finish, we measured the cells 3 month (90 days) after their fabrication. We stored them at ambient light under inert atmosphere and observed a slight loss of efficiency of 1–3% for *o*-xylene processed devices but almost 20% loss with the chlorobenzene-processed active layer. This observation highlights another benefit of using *o*-xylene instead of chlorobenzene for the deposition of the active layers.

Conclusions

We designed and synthetised a star-shape non fullerene acceptor based on an aza-triangulene core. This molecule showed

good solubility in chlorinated and especially non-chlorinated solvents. **AzaTk** shows a broad absorption in the visible range with an additional band around 500 nm corresponding to the HOMO−1 → LUMO transition. We characterized the **AzaTk** crystal structure and showed that the stiffening of the core leads to an increase in the steric hindrance around the central nitrogen atom. We also highlighted the good π–π stacking interaction stacking distance on the fluorine acceptor parts of the molecule. Energy levels lie at −5.3 eV for the HOMO and −4.2 eV for the LUMO which is suitable for blending with PTB7-Th donor polymer. Interestingly, electron mobility of pristine **AzaTk** deposited in *o*-xylene and chlorobenzene are quite similar (respectively 1.13–2.15 × 10^{-4} and 1.23–2.70 × 10^{-4} cm^2 V^{-1} s^{-1}) and are not significantly affected by thermal annealing indicating the minor influence of **AzaTk** organisation. This properties of the star-shape structure favours the simple as-cast process essential for industrial scale-up. Photovoltaic properties were evaluated by blending them with PTB7-Th donor polymer. Small differences are observed between both solvents leading to an efficiency of 6.46% in chlorobenzene and 6.27% in *o*-xylene. Both devices show a very similar morphological structure which demonstrates the benefit of using non-halogenated solvent. Moreover, similar recombination properties were found for both types of devices, which confirms the identical V_{OC} values reported for the JV curve. On the other hand, the faster electronic transport observed in impedance spectroscopy in the *o*-xylene based devices could explain the slightly higher J_{SC}.

Interestingly, **AzaTk** shows better photochemical stability than the reference ITIC making star-shape molecules potential candidates for the fabrication of solar cells as cast and without halogenated solvents. Degradation mechanism was confirmed and this result tends to indicate that the protection of the β-position of the lateral thiophene is essential to improve the photostability of next generation NFAs. Further investigations will take account of this behaviour for the design of NFA molecules.

We demonstrated with this work that star-shape molecules based on aza-triangulene core can be used as NFA deposited from more industrial friendly solvents, without post-treatment with the same level of performance as classical procedure.

Author contributions

Y. K. synthesized the intermediate molecules and the NFA. Y. K. and J. M. A. C. performed the optoelectronic characterizations and the theoretical modelling of **AzaTk**. Y. A. A. Q., Q. E., A. K. and C. V. A. developed, fabricated and characterized the OSCs and the OTFTs and optimized the devices. Y. A. A. Q., A. R. and J. A. designed and performed the photo-degradation study. J. P. performed the RX diffraction. C. A. and B. G. performed and analyzed the AFM measurements. T. K. and N. Y. have analyzed the blends with 2D-GIXD technique and A. J. R. and V. M. measured and analyzed the devices with impedance spectroscopy. J. A., R. D. and C. A. designed the experiments and the molecules. C. A. supervised the work, provided interpretation of experimental data, and wrote the final manuscript including the contributions of all coauthors. All the authors contributed to the preparation of the manuscript and ESI.†

Conflicts of interest

There are no conflicts to declare.

Acknowledgements

This project has received funding by the French Research Agency (project ANR-17-CE05-0020-01 named NFA-15). AK received funding from the framework of a CIFRE PhD grant 2020/0978 to AK from the ANRT (Association Nationale de la Recherche et de la Technologie) and the Ministère de l'Enseignement Supérieur, de la Recherche et de l'Innovation, awarded through the company Dracula Technologies (Valence, France). QE and CVA received funding from the French Research Agency (project ANR-18-CE04-0007-04 named BELUGA). The synchrotron radiation experiments were performed at BL19B2 in SPring-8 with the approval of Japan Synchrotron Radiation Research Institute (JASRI) (Proposal No. 2018B1791 and 2019B1851). R. D., A. J. R., J. M. A. C. and V. M. acknowledges the European Research Council (ERC) for funding. This work was partially funded under the European Union's Horizon 2020 research and innovation (grant agreement number 832606; project PISCO). C. A. thank the financial support of the CEA Exploratory Programme 2022 ''PHOTENER''.

Notes and references

1 O. Inganäs, *Adv. Mater.*, 2018, **30**, 1800388.
2 C. Yan, J. Qin, Y. Wang, G. Li and P. Cheng, *Adv. Energy Mater.*, 2022, **12**, 2201087.
3 B. Zheng, L. Huo and Y. Li, *NPG Asia Mater.*, 2020, **12**, 1–22.
4 R. A. J. Janssen and J. Nelson, *Adv. Mater.*, 2013, **25**, 1847–1858.
5 D. Luo, W. Jang, D. D. Babu, M. S. Kim, D. H. Wang and A. K. K. Kyaw, *J. Mater. Chem. A*, 2022, **10**, 3255–3295.
6 Y. Lin, Y. Firdaus, M. I. Nugraha, F. Liu, S. Karuthedath, A.-H. Emwas, W. Zhang, A. Seitkhan, M. Neophytou, H. Faber, E. Yengel, I. McCulloch, L. Tsetseris, F. Laquai and T. D. Anthopoulos, *Adv. Sci.*, 2020, **7**, 1903419.
7 Y. Han, H. Dong, W. Pan, B. Liu, X. Chen, R. Huang, Z. Li, F. Li, Q. Luo, J. Zhang, Z. Wei and C.-Q. Ma, *ACS Appl. Mater. Interfaces*, 2021, **13**, 17869–17881.
8 Y. A. Avalos-Quiroz, O. Bardagot, Y. Kervella, C. Aumaître, L. Cabau, A. Rivaton, O. Margeat, C. Videlot-Ackermann, U. Vongsaysy, J. Ackermann and R. Demadrille, *ChemSusChem*, 2021, **14**, 3502–3510.
9 R. Sun, W. Wang, H. Yu, Z. Chen, X. Xia, H. Shen, J. Guo, M. Shi, Y. Zheng, Y. Wu, W. Yang, T. Wang, Q. Wu, Y. (Michael) Yang, X. Lu, J. Xia, C. J. Brabec, H. Yan, Y. Li and J. Min, *Joule*, 2021, **5**, 1548–1565.
10 P. Xue, P. Cheng, R. P. S. Han and X. Zhan, *Mater. Horiz.*, 2022, **9**, 194–219.

11 K. Chong, X. Xu, H. Meng, J. Xue, L. Yu, W. Ma and Q. Peng, *Adv. Mater.*, 2022, **34**, 2109516.
12 Y. Cui, Y. Xu, H. Yao, P. Bi, L. Hong, J. Zhang, Y. Zu, T. Zhang, J. Qin, J. Ren, Z. Chen, C. He, X. Hao, Z. Wei and J. Hou, *Adv. Mater.*, 2021, **33**, 2102420.
13 H. Meng, C. Liao, M. Deng, X. Xu, L. Yu and Q. Peng, *Angew. Chem., Int. Ed.*, 2021, **60**, 22554–22561.
14 X. Xu, L. Yu, H. Meng, L. Dai, H. Yan, R. Li and Q. Peng, *Adv. Funct. Mater.*, 2022, **32**, 2108797.
15 W. Li, D. Liu and T. Wang, *Adv. Funct. Mater.*, 2021, **31**, 2104552.
16 J. Luke, E. M. Speller, A. Wadsworth, M. F. Wyatt, S. Dimitrov, H. K. H. Lee, Z. Li, W. C. Tsoi, I. McCulloch, D. Bagnis, J. R. Durrant and J.-S. Kim, *Adv. Energy Mater.*, 2019, **9**, 1803755.
17 X. Gu, Y. Zhou, K. Gu, T. Kurosawa, Y. Guo, Y. Li, H. Lin, B. C. Schroeder, H. Yan, F. Molina-Lopez, C. J. Tassone, C. Wang, S. C. B. Mannsfeld, H. Yan, D. Zhao, M. F. Toney and Z. Bao, *Adv. Energy Mater.*, 2018, **7**, 1602742.
18 J. Zhang, Y. Li, J. Huang, H. Hu, G. Zhang, T. Ma, P. C. Y. Chow, H. Ade, D. Pan and H. Yan, *J. Am. Chem. Soc.*, 2017, **139**, 16092–16095.
19 X. Wu, W. Wang, H. Hang, H. Li, Y. Chen, Q. Xu, H. Tong and L. Wang, *ACS Appl. Mater. Interfaces*, 2019, **11**, 28115–28124.
20 S. K. Pathak, H. Liu, C. Zhou, G. Xie and C. Yang, *J. Mater. Chem. C*, 2021, **9**, 7363–7373.
21 R. Xiao, Y. Xiang, X. Cao, N. Li, T. Huang, C. Zhou, Y. Zou, G. Xie and C. Yang, *J. Mater. Chem. C*, 2020, **8**, 5580–5586.
22 Y.-Q. Pan and G.-Y. Sun, *ChemSusChem*, 2019, **12**, 4570–4600.
23 M. Wu, J.-P. Yi, L. Chen, G. He, F. Chen, M. Y. Sfeir and J. Xia, *ACS Appl. Mater. Interfaces*, 2018, **10**, 27894–27901.
24 P. Cheng, X. Zhao and X. Zhan, *Acc. Mater. Res.*, 2022, **3**, 309–318.
25 M. Wu, J.-P. Yi, J. Hu, P. Xia, H. Wang, F. Chen, D. Wu and J. Xia, *J. Mater. Chem. C*, 2019, **7**, 9564–9572.
26 W. Wang, X. Wu, H. Hang, H. Li, Y. Chen, Q. Xu, H. Tong and L. Wang, *Chem. – Eur. J.*, 2019, **25**, 1055–1063.
27 K. Lin, B. Xie, Z. Wang, R. Xie, Y. Huang, C. Duan, F. Huang and Y. Cao, *Org. Electron.*, 2018, **52**, 42–50.
28 W. Wu, G. Zhang, X. Xu, S. Wang, Y. Li and Q. Peng, *Adv. Funct. Mater.*, 2018, **28**, 1707493.
29 X. Liao, Q. Xie, Y. Guo, Q. He, Z. Chen, N. Yu, P. Zhu, Y. Cui, Z. Ma, X. Xu, H. Zhu and Y. Chen, *Energy Environ. Sci.*, 2022, **15**, 384–394.
30 H. Jiang, N. Lai, J. Tang, X. Tian, F. Wei, W. Bai and Y. Xu, *J. Photochem. Photobiol., A*, 2019, **369**, 195–201.
31 Y. Xiong, B. Wu, X. Zheng, Z. Zhao, P. Deng, M. Lin, B. Tang and B. S. Ong, *Adv. Sci.*, 2017, **4**, 1700110.
32 W. Song and J. Y. Lee, *Adv. Opt. Mater.*, 2017, **5**, 1600901.
33 J. S. Ward, N. A. Kukhta, P. L. dos Santos, D. G. Congrave, A. S. Batsanov, A. P. Monkman and M. R. Bryce, *Chem. Mater.*, 2019, **31**, 6684–6695.
34 T. A. Schaub, T. Mekelburg, P. O. Dral, M. Miehlich, F. Hampel, K. Meyer and M. Kivala, *Chem. – Eur. J.*, 2020, **26**, 3264–3269.
35 Y. N. Luponosov, A. N. Solodukhin, A. L. Mannanov, P. S. Savchenko, Y. Minenkov, D. Y. Paraschuk and S. A. Ponomarenko, *Dyes Pigm.*, 2020, **177**, 108260.
36 S. Paek, N. Cho, S. Cho, J. K. Lee and J. Ko, *Org. Lett.*, 2012, **14**, 6326–6329.
37 S. Paek, H. Choi, J. Sim, K. Song, J. K. Lee and J. Ko, *J. Phys. Chem. C*, 2014, **118**, 27193–27200.
38 D.-X. Zhao, L.-Y. Bian, Y.-X. Luo, M.-D. Zhang, H. Cao and M.-D. Chen, *Dyes Pigm.*, 2017, **140**, 278–285.
39 J. Wan, L. Zeng, X. Liao, Z. Chen, S. Liu, P. Zhu, H. Zhu and Y. Chen, *Adv. Funct. Mater.*, 2022, **32**, 2107567.
40 J. Yuan, Y. Zhang, L. Zhou, G. Zhang, H.-L. Yip, T.-K. Lau, X. Lu, C. Zhu, H. Peng, P. A. Johnson, M. Leclerc, Y. Cao, J. Ulanski, Y. Li and Y. Zou, *Joule*, 2019, **3**, 1140–1151.
41 Y. Yang, Z.-G. Zhang, H. Bin, S. Chen, L. Gao, L. Xue, C. Yang and Y. Li, *J. Am. Chem. Soc.*, 2016, **138**, 15011–15018.
42 J. Fang, Z. Wang, Y. Chen, Q. Zhang, J. Zhang, L. Zhu, M. Zhang, Z. Cui, Z. Wei, H. Ade and C.-Q. Ma, *Cell Rep. Phys. Sci.*, 2022, **3**, 100983.
43 Z. Li, X. Xu, W. Zhang, X. Meng, W. Ma, A. Yartsev, O. Inganäs, M. R. Andersson, R. A. J. Janssen and E. Wang, *J. Am. Chem. Soc.*, 2016, **138**, 10935–10944.
44 W. Li, M. Chen, J. Cai, E. L. K. Spooner, H. Zhang, R. S. Gurney, D. Liu, Z. Xiao, D. G. Lidzey, L. Ding and T. Wang, *Joule*, 2019, **3**, 819–833.
45 R. Singh, J. Lee, M. Kim, P. E. Keivanidis and K. Cho, *J. Mater. Chem. A*, 2016, **5**, 210–220.
46 A. Mahmood and J.-L. Wang, *Sol. RRL*, 2020, **4**, 2000337.
47 T. Kuwabara, M. Nakamoto, Y. Kawahara, T. Yamaguchi and K. Takahashi, *J. Appl. Phys.*, 2009, **105**, 124513.
48 T. Kuwabara, Y. Kawahara, T. Yamaguchi and K. Takahashi, *ACS Appl. Mater. Interfaces*, 2009, **1**, 2107–2110.
49 G. Garcia-Belmonte, A. Munar, E. M. Barea, J. Bisquert, I. Ugarte and R. Pacios, *Org. Electron.*, 2008, **9**, 847–851.
50 S. Züfle, S. Altazin, A. Hofmann, L. Jäger, M. T. Neukom, W. Brütting and B. Ruhstaller, *J. Appl. Phys.*, 2017, **122**, 115502.
51 L. Ke, N. Zhang, E. Low, R. Wang, Z. M. Kam, X. Wang, B. Liu and J. Zhang, *Sol. Energy*, 2017, **144**, 367–375.
52 M. Knipper, J. Parisi, K. Coakley, C. Waldauf, C. J. Brabec and V. Dyakonov, *Z. Naturforsch., A: Phys. Sci.*, 2007, **62**, 490–494.
53 B. Xiao, M. Zhang, J. Yan, G. Luo, K. Gao, J. Liu, Q. You, H.-B. Wang, C. Gao, B. Zhao, X. Zhao, H. Wu and F. Liu, *Nano Energy*, 2017, **39**, 478–488.
54 B. Yang, Y. Yuan and J. Huang, *J. Phys. Chem. C*, 2014, **118**, 5196–5202.
55 T. M. Clarke, C. Lungenschmied, J. Peet, N. Drolet and A. J. Mozer, *Adv. Energy Mater.*, 2015, **5**, 1401345.
56 F. Fabregat-Santiago, G. Garcia-Belmonte, I. Mora-Seró and J. Bisquert, *Phys. Chem. Chem. Phys.*, 2011, **13**, 9083–9118.
57 M. Glatthaar, M. Riede, N. Keegan, K. Sylvester-Hvid, B. Zimmermann, M. Niggemann, A. Hinsch and A. Gombert, *Sol. Energy Mater. Sol. Cells*, 2007, **91**, 390–393.
58 G. Schlichthorl, N. G. Park and A. J. Frank, *J. Phys. Chem. B*, 1999, **103**, 782–791.
59 S. Park and H. J. Son, *J. Mater. Chem. A*, 2019, **7**, 25830–25837.
60 Y. Che, M. R. Niazi, R. Izquierdo and D. F. Perepichka, *Angew. Chem., Int. Ed.*, 2021, **60**, 24833–24837.